LONGITUDINAL INSTABILITY ANALYSIS FOR THE IPNS UPGRADE *

K. Harkay, Y. Cho, E. Lessner, Argonne National Laboratory, Argonne, IL 60439 USA

Abstract

The proposed 1-MW spallation neutron source upgrade calls for a 2-GeV rapidly-cycling synchrotron (RCS) with an intensity of 1.04×10^{14} protons per pulse [1]. Due to the high intensity, the potential exists for collective instabilities. Emphasis is placed on controlling these by (a) minimizing the machine impedance by using a contour-following rf shield and (b) maximizing the momentum spread to make use of Landau damping. The coupling impedance is estimated and is dominated by space charge effects. It is found that the longitudinal microwave stability limit can be exceeded unless the momentum spread is sufficient. A longitudinal tracking code was developed to simulate injection and acceleration, including the effects of space charge and other sources of impedance [2]. With the aid of the simulation, and under the assumptions of the instability theory, we arrive at an rf voltage profile and beam injection parameters which avoid both the instability and beam loss through the entire cycle. The limitations of the analysis are explored.

I. INTRODUCTION

Of the several known longitudinal instabilities, only the single-bunch instabilities need to be considered since the RCS operates with a harmonic number $h=1$. The microwave instability is potentially the most dangerous, and it is analyzed in detail. This instability should not occur in a machine operating below transition energy, such as the RCS, if the coupling impedance is purely capacitive (space charge). However, it could occur in the RCS when there are resistive components. The instability growth rate then depends on the momentum distribution of the beam, particularly the shape of the distribution tails. A detailed analysis of this instability requires not only knowledge of the coupling impedance seen by the beam, but also the peak current and energy spread of the beam. At this stage, this beam information was obtained through Monte Carlo simulations [2].

A conservative approach is adopted to prevent the onset of instability:
- The contributions to the coupling impedance from the various RCS components are estimated.
- The Keil-Schnell criterion, modified for bunched beams, is used to obtain the $\Delta p/p$ required to raise the threshold current, although it overestimates the severity of the instability below transition energy.
- Using the peak current and energy spread of the circulating beam obtained from the longitudinal tracking studies, a detailed analysis of the stability diagram is made.

II. COUPLING IMPEDANCE ESTIMATION

The longitudinal coupling impedance, $Z_{\parallel}$, is estimated using the standard approximations [3-5]. The impedance for the RCS is dominated by space charge effects. The beam position monitors (BPMs), rf cavities, and the rf shield also contribute to the impedance. The contribution of the extraction kickers is negligible. The impedance due to other components, such as vacuum ports and bellows, is expected to be negligible because these are isolated from the beam by the rf shield.

The results for the longitudinal coupling impedance are summarized in Table 1. The impedance is normalized by the mode numbers, $n = \omega/\omega_0$, where ω_0 is the revolution frequency (1.1 to 1.5 MHz). The coupling impedance of interest corresponds to the mode numbers $n \leq 500$, using the cutoff frequency $\omega_c = c/b$, where b is the rf shield radius and c is the velocity of light. The results in the table correspond to injection energy (400 MeV), unless otherwise noted. The space charge impedance is purely capacitive, while the others are inductive, and include a resistive term.

Table 1: RCS Longitudinal Impedance Estimation (at ω_c)

	$\mathrm{Re}\left(Z_{\parallel}/n\right)$ (Ω)	$\mathrm{Im}\left(Z_{\parallel}/n\right)$ (Ω)
Space charge (injection)	–	-220
Space charge (extraction)	–	-50
Rf shield	0.01	0.01
Rf cavities	14 **	†
BPMs ††	0.1	0.06

**   decreasing to zero at $\omega \ll \omega_c$ and $\omega \gg \omega_c$

†   inductive for $\omega < \omega_c$, capacitive for $\omega > \omega_c$

††   valid up to 125 MHz

The impedance due to the rf cavity higher-order modes (HOMs) was found using URMEL-T [1]. The calculations correspond to a fundamental frequency of 1.3 MHz, which is about midway through the acceleration cycle and for which the ratio R_{sh}/Q is found to be 105. The frequencies and R_{sh}/Q for the first few HOMs are listed in Table 2. The value of 14 Ω for the rf cavities listed in Table 1 is the rf-equivalent broadband impedance ($Q = 1$) and corresponds to 10 cavities.

Table 2: Ratio of Shunt Impedance and Q
of First Few HOMs for an RF Cavity

$\omega_{\mathrm{res}}/2\pi$ (MHz)	R_{sh}/Q (Ω)
5.6	5.5
10.5	0.8
14.8 ***	0.2

*** Extrapolation of ferrite properties beyond normal operating range of 0.5 to 10 MHz.

To minimize the impedance due to space charge, the vacuum chamber is constructed with a special rf shield, shown

in Figure 1. The shield consists of Be-Cu wires which follow the beam envelope at an aperture equal to the beam-stay-clear (BSC), given by $A = \sqrt{2\beta\varepsilon/\pi} + |\eta_D \, \Delta p/p| + \text{COD}$, where β is the lattice function, $\varepsilon = 375\pi$ mm-mr is the beam emittance, η_D is the dispersion function, and COD is the closed orbit distortion (≤ 1 mm). The space charge impedance is calculated using the standard assumption of a uniform, round, unbunched beam of radius a in a vacuum chamber of radius b. The geometrical factor is given by $g_0 = 1 + 2\ln(b/a)$ [3,4]. Compared to a fixed-radius rf shield, this contour-following scheme reduces the longitudinal space charge impedance by 30% at injection and 20% at extraction.
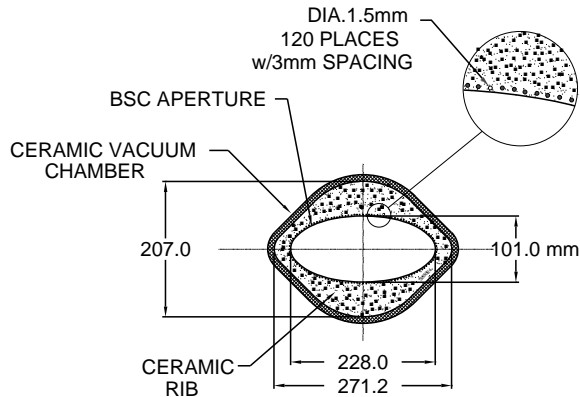

Figure 1: Ceramic vacuum chamber cross section in the focusing quadrupole magnet.

A number of corrections to the geometrical factor have been proposed to account for the wires and the more realistic elliptical beam cross-section. The electrostatic fields due to a uniform beam propagating inside a round rf-screening wire cage have been derived by T. Wang [6]. A second correction, derived by H. Okamoto, takes into account the varying elliptical shape of beam in a smooth, metallized vacuum chamber without wires and with a fixed radius [7]. These corrections result in a difference of less than 2% in the longitudinal impedance, and can be neglected [8].

III. STABILITY CRITERION

A simplified criterion for the longitudinal stability threshold, commonly referred to as the Keil-Schnell (K–S) criterion, is independent of the details of the particle phase space distribution and is given by [3,4]

$$\left|\frac{Z_\parallel}{n}\right| \leq F \frac{|\eta|\beta^2 \, E/e}{I_{pk}} \left(\frac{\Delta p_{\text{FWHM}}}{p}\right)^2, \tag{1}$$

where local values of the current and momentum are used for bunched beams. Here $F \approx 1$ is a form factor, I_{pk} is the peak current, and η is the slip factor.

The K–S criterion imposes a lower bound on the ratio $(\Delta p)^2/I_{pk}$. For a given bunch area, increasing the momentum spread is more effective in achieving stability than is lowering

the peak current. Therefore, the stability requirement drives the peak rf voltage. The optimal injected beam parameters and rf voltage profile through the cycle are obtained through the simulation studies [2]. The injected beam is chopped, with an energy spread of ±2.5 MeV and a length of 75% of the circumference. The time-varying peak current, obtained from the simulation, and the rf voltage are shown in Figure 2a.

The momentum spread corresponding to the threshold for the microwave instability is computed by substituting the impedance listed in Table 1 and the peak current from Figure 2a into Eq. (1). The time-variation in the threshold momentum spread is plotted in Figure 2b together with the momentum spread obtained from the simulation. The beam remains in the stable region through the cycle. The requirement that beam losses be less than 0.1% is also met.
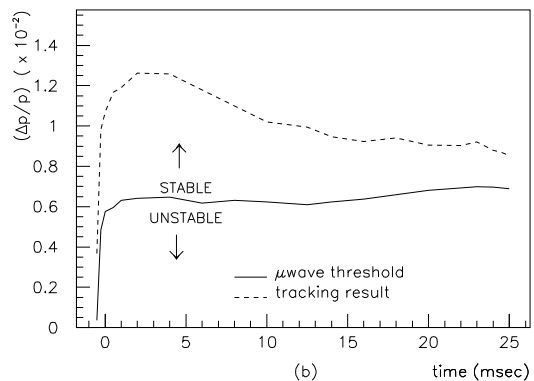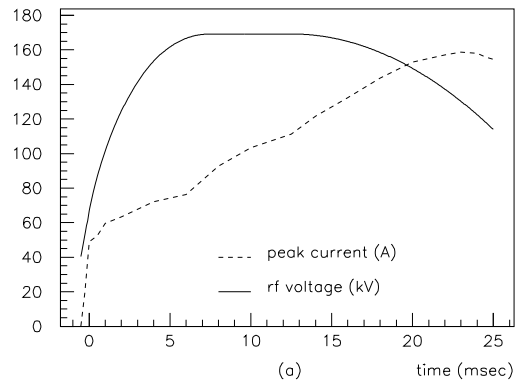

Figure 2: (a) Variation of the rf voltage and peak current and (b) threshold $\Delta p/p$ compared to that obtained from tracking. The small variations are due to the Monte Carlo statistics.

IV. STABILITY DIAGRAM

Below transition, it is possible to operate the machine outside the K–S boundary and preserve stability. The stable region is dependent on both the resistive component of the impedance and the shape of the distribution tails. The details are discussed below.

The response of a beam to a periodic perturbation, $\exp(j(\Omega t - n\varphi))$, is given by the Vlasov equation, where φ is the azimuthal phase coordinate and Ω is the driving frequency of the perturbation. The solution to the small-amplitude Vlasov equation leads to a dispersion relation, which, for a coasting beam, is given by [9]

$$1 = -\frac{2}{\pi}\frac{I}{(E/e)\beta^2|\eta|(\Delta p/p)^2}\frac{Z_\parallel}{n}I_D'. \qquad (2)$$

I_D' is the normalized dispersion integral, given by

$$I_D' = j\int\frac{\partial f/\partial x}{x - x_1}dx,$$

where $x = (n\omega - n\omega_0)/(nS)$, $x_1 = (\Omega - n\omega_0)/(nS)$, the full spread at half maximum of the revolution frequency distribution is given by $2S = -\eta\omega_0(\Delta p/p)$, and $f(x)$ is the normalized beam density distribution in frequency space. The imaginary part of the driving frequency leads to growth of the perturbation. A finite spread in the revolution frequency or, equivalently, in momentum, gives rise to Landau damping. The stability boundary is obtained using Eq. (2) evaluated with $\mathrm{Im}\,\Omega = 0$.

The stability diagram for the RCS at 2 GeV is plotted in Figure 3a in the impedance plane for the quartic momentum spread shown in Figure 3b. Also shown in Figure 3a is the stability region which satisfies the K–S criterion. The positive vertical axis denotes capacitive impedance, and the longitudinal coupling impedance listed in Table 1 is plotted near the vertical axis as a large dot. The particle momentum distribution in Figure 3b is obtained from the simulation.

The stability boundary depends specifically on the momentum distribution and can give a higher limit than the K–S criterion. However, the upper portion of the stability boundary, which corresponds to the tails of the distribution, is highly sensitive to the beam distribution. This can be seen in Figure 4a, which shows the stability boundary using a different, smoothed distribution, shown in Figure 4b. Sections of the stability diagram are marked according to the corresponding section of the momentum distribution. Experience shows that in measured data, the tails in the line density can be rather unpredictable.

The RCS is dominated by the capacitive space charge impedance, which then determines the resistive $\mathrm{Re}(Z_\parallel/n)$ limit for stability. The stable boundary satisfying the K–S criterion in Figure 3a suggests that the beam is stable at 2 GeV to a threshold $\mathrm{Re}(Z_\parallel/n)$ of 70 Ω. This can readily be achieved in the RCS. A similar analysis at 400 MeV gives a resistive limit of 550 Ω. The stability criterion is most critical near extraction because the peak current increases by a factor of five, while the momentum spread decreases by 30%.

V. DISCUSSION

The microwave instability is avoided in the RCS by ensuring that the coupling impedance is within the stable region defined by the K-S criterion. This conclusion is valid within the assumptions of the theory and the impedance estimate. Rigid, longitudinal displacements of the bunch and possible emittance growth could occur in the latter part of the cycle, such as due to a fixed-frequency rf cavity HOM not analyzed by URMEL-T. The rf bucket produced by the rf voltage in Figure 2a grows significantly after the midpoint in the cycle, and would be sufficient to contain the bunch. Also,
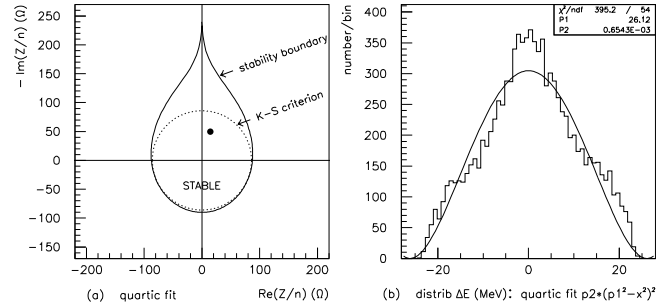

Figure 3: Longitudinal stability boundary (a) for a quartic momentum distribution (b).
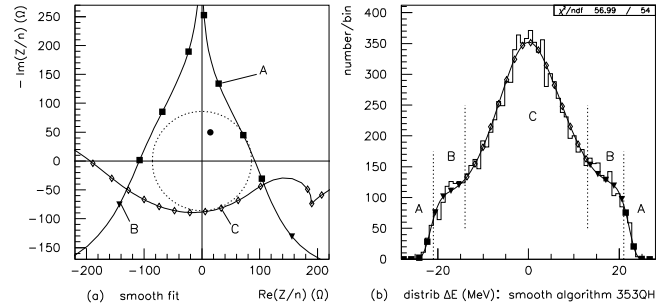

Figure 4: Dependence of the longitudinal stability boundary (a) on momentum distribution, using the distribution in (b).

active control is provided by the phase feedback system of the RCS rf system.

VI. REFERENCES

[1] "IPNS Upgrade: A Feasibility Study," ANL-95/13, (April 1995).

[2] Y. Cho, E. Lessner, K. Symon, "Injection and Capture Simulations for a High Intensity Proton Synchrotron, *Proc. of EPAC*, 1228, (1994).

[3] V.K. Neil and A.M. Sessler, "Longitudinal Resistive Instabilities of Intense Coasting Beams in Particle Accelerators," *Rev. Sci. Instrum.*, **36** (4), 429, (1965).

[4] E. Keil and W. Schnell, "Concerning Longitudinal Stability in the ISR," CERN TH-RF/69-48, (1969).

[5] K.-Y. Ng, "Fields, Impedances, and Structures," *The Physics of Particle Accel.*, AIP Conf. Proc. 184, (1989).

[6] T-S. F. Wang, "Electrostatic Field of a Perturbed Beam with RF-Screening Wires," CERN/PS 94-08 (DI), (1994).

[7] "AUSTRON Accelerator Feasibility Study," AUSTRON/PS/PJB, Chapter 4, p. 145, (October 1994).

[8] K.C. Harkay, "Study of Corrections to the Geometrical Factor in the Space Charge Impedance for the IPNS Upgrade," ANL Report NS-95-4, (March 1995).

[9] A. Hoffman, "Single-beam collective phenomena – longitudinal," *Proc. of Theoretical Aspects of the Behavior of Beams in Accel. and Storage Rings*, CERN 77-13, (November 1976).